*Manuscript
Click here to view linked References

Double Photon Emission Coincidence Imaging with GAGG-SiPM Compton Camera

Mizuki Uenomachi[a,*], Yuki Mizumachi[a], Yuri Yoshihara[a], Hiroyuki Takahashi[a], Kenji Shimazoe[a], Goro Yabu[b], Hiroki Yoneda[b], Shin Watanabe[b], Shin'ichiro Takeda[c], Tadashi Orita[c], Tadayuki Takahashi[b,c], Fumiki Moriyama[d], Hirotaka Sugawara[d]

[a]*Department of Nuclear Engineering and Management, The University of Tokyo, 7-3-1, Bunkyo-ku, Tokyo, Japan*
[b]*Department of Physics, The University of Tokyo, 7-3-1, Bunkyo-ku, Tokyo, Japan*
[c]*Kavli IPMU, The University of Tokyo, 5-1-5, Kashiwanoha, Kashiwa, Chiba, Japan*
[d]*Okinawa Institute of Science and Technology Graduate University, 1919-1, Tancha, Onna-son, Kunigami-gun, Okinawa, Japan*

Abstract

A Compton camera is a promising gamma-ray imaging method based on Compton scattering kinetics due to the high Compton scattering probability for sub-MeV gamma-rays. The conventional Compton camera has a disadvantage of low signal-to-ration (SNR), which is caused by the drawing of multiple Compton cones. A method to solve this fundamental problem is double-photon emission computed tomography (DPECT), which uses the coincidence detection for cascade gamma-rays and significantly increases the SNR using intersection of two Compton cones. In this study, we demonstrated the DPECT method for ^{134}Cs imaging, which is one of important radioisotopes for the imaging of fuel debris, with two Ce:$Gd_3(Al,Ga)_5O_{12}$ (GAGG) scintillator Compton cameras.

Keywords: Compton camera, Double photon emission coincidence imaging, Compton imaging, Caesium-134

1. Introduction

A Compton Camera is a promising gamma-ray imaging method based on Compton scattering kinetics due to the high Compton scattering probability for sub-MeV gamma-rays [1]. It has the advantages of being light weight and has a wide field of view compared with mechanically collimated camera with thick collimators when used in sub-MeV gamma-ray imaging [2]. Several groups have developed Compton imagers recently for visualizing radioisotopes such as ^{137}Cs and ^{134}Cs, which are environmentally distributed by the accident in Fukushima [3, 4, 5]. However, a three-dimensional gamma-ray imaging is strongly required for the assessment of fuel debris and nuclear wastes. The realization of effective images with high signal-to-noise ratio (SNR) in Compton imaging is still under investigation. One of the drawbacks of Compton-imaging is the low SNR caused by the drawing of multiple Compton cones, which render it difficult to apply the Compton camera to distributed source imaging.

Several methods can be used to solve the fundamental problem in Compton imaging. One of methods is to recoil the electron tracking in Compton camera, which uses information of recoiled electron track, and the probability from one event is limited from cones to arcs [6]. Electron-tracking Compton imaging using a solid detector is now under investigation [7, 8, 9] as it requires sub-10 μm position resolution and timing information.

Another method is double-photon emission computed tomography (DPECT), which uses the coincidence detection for cascade gamma-rays and significantly increases the SNR using the intersection of two Compton cones. If two cascade gamma-rays, released from a single isotope with a short delay, are detected by multiple Compton cameras, the source point could be estimated by using the intersection of Compton cones. Thes initial investigation of DPECT using GEANT4 simulation has been reported in a previous study [10]; it showed a significant improvement in the SNR compared with single Compton imaging. For the imaging of fuel debris, for example, ^{134}Cs and ^{60}Co are important

*Corresponding author
Email address: uenomachi-mizuki0710@g.ecc.u-tokyo.ac.jp (Mizuki Uenomachi)

© 2020. This manuscript version is made available under the CC-BY-NC-ND 4.0 license http://creativecommons.org/licenses/by-nc-nd/4.0/

key elements that release two or more cascade gamma-rays with a short delay. ^{134}Cs emits primarly two gamma-rays of 796 keV and 605 keV, and ^{60}Co emits two gamma-rays of 1173 keV and 1333 keV like Fig.2. Therefore, this method could be applied for the imaging of fuel debris. In this study, we dperformed the experiment of DPECT imaging for ^{134}Cs.

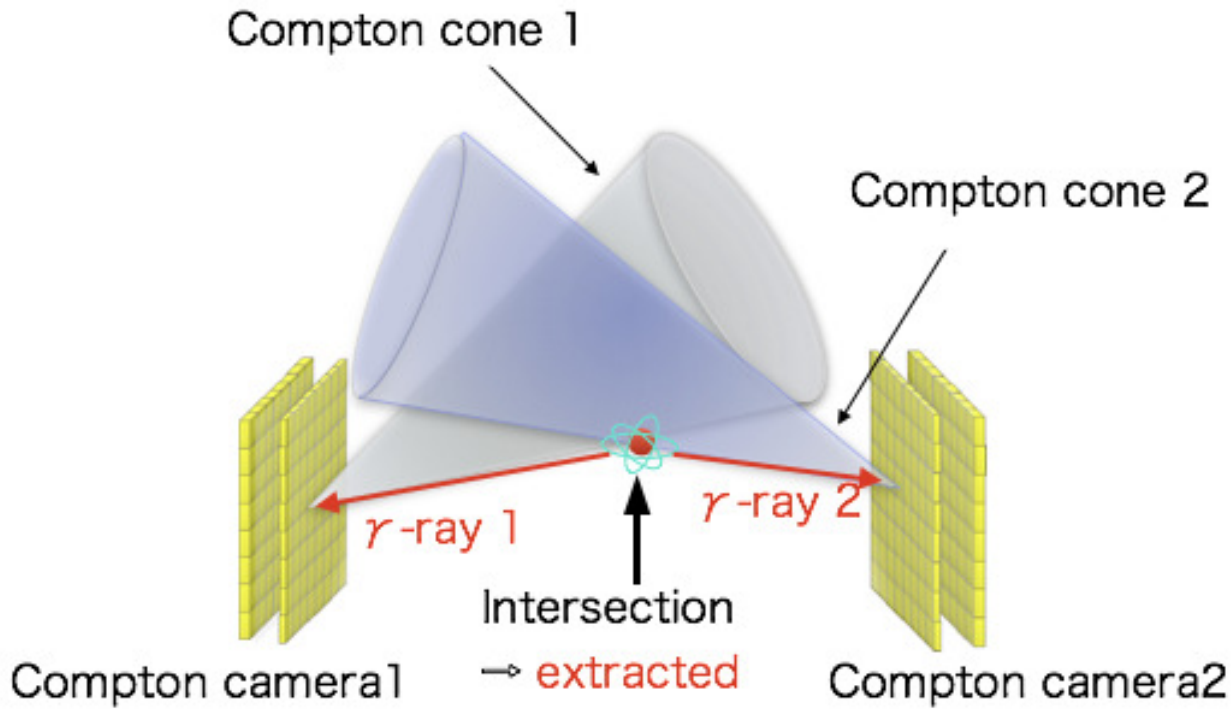

Figure 1: Principle of DPECT. The coincidence detection for cascade gamma-rays increases the SNR using the intersection of two Compton cones.

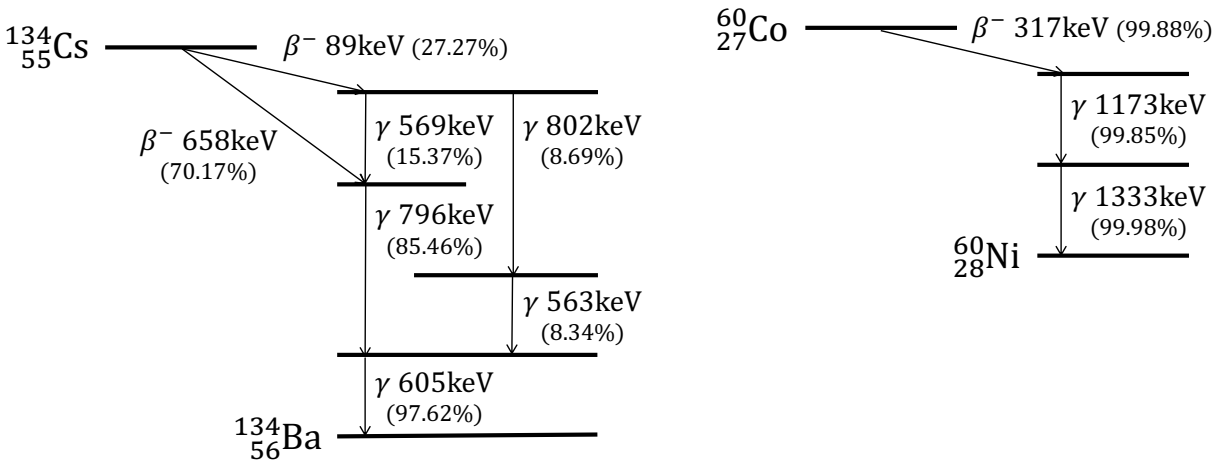

Figure 2: The decay scheme of ^{134}Cs and ^{60}Co.

2. Materials and Methods

2.1. Experimental setup

For the application of fuel debris, our group have developed an 8 × 8 Ce:$Gd_3(Al,Ga)_5O_{12}$ (GAGG) scintillator Compton camera [3, 4]. Ce:GAGG has good characteristics of high light yields (∼ 46,000 photons/MeV), high density (∼ 6.63 g/cm^3), high atomic number (Z = 54), and non-deliquescence [11]. We used two GAGG scintillator Compton cameras for the DPECT experiment (camera1, camera2). The Compton camera consists of a scatter layer and an absorber layer, and the scatter and absorber of camera1 and the absorber of camera2 is an 8 × 8 array (64 crystals). The scatter of camera1 is a 6 ×7 array (42 crystals) because the Ce:GAGG crystals and SiPM are shortage. The size of the Ce:GAGG detector in the scatter is 10 mm × 10 mm × 5 mm, and that in the absorber is 10 mm × 10 mm × 10 mm. Each of the Ce:GAGG scintillators is coupled to a silicon photo multiplier (SiPM, KETEK PM6660). Signals with pulse height information from each SiPM are converted to digital signals with time width information by the dynamic Time-over-Threshold (dToT) method [12, 13] in parallel. These data are acquired by a field-programmable gate-array (FPGA, Xilinx inc. XC7K70T-1FBG484C) based 144 chnnel data acquisition (DAQ) board. The channel number, time stamp, and time width are recorded in a binary file with a 2.5 ns clock for each event. The energy resolution of camera1 and camera2 are 12.41 % and 12.42 % for 662 keV, respectively. In the DPECT experiment, two DAQ boards were used for camera1 and camera2. To synchronize the two DAQ boards, 50 ms external clocks generated by a function generator were input to the two DAQ boards.

Figure 3 shows the experimental setup of DPECT. Two Compton cameras were arranged in opposite directions at 120 mm apart (corresponding to the distance from the surface of camera1box to that of camera2 box). The distance from the scatterer to the absorber was 109 mm, and that from the surface of the box to the surface of the scatterer was 10 mm .

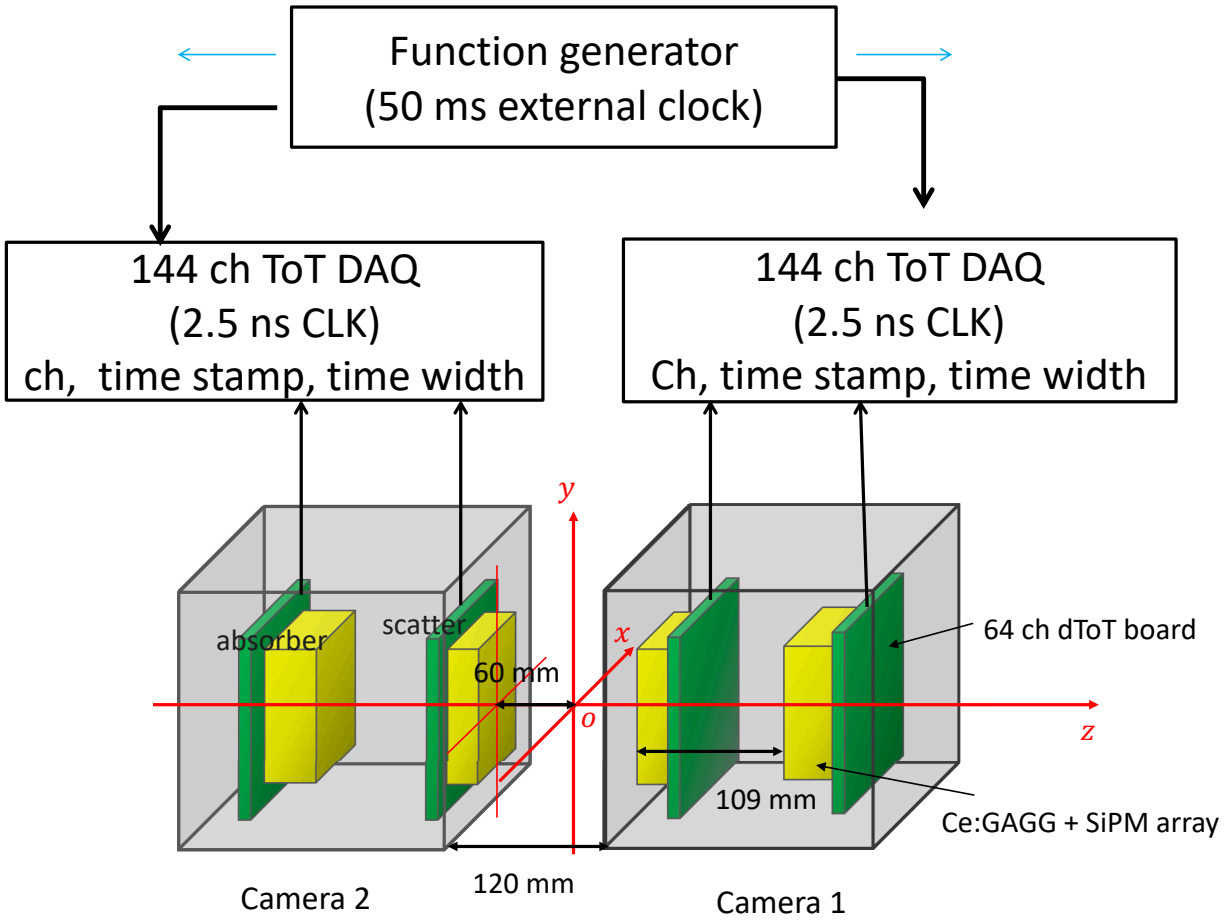

Figure 3: Experimental setup of DPECT. Two Compton cameras were arranged in opposite directions at a distance of 120 mm.

2.2. *Data analysis*

The data analysis flow is shown in Fig.4. First, coincidence events of the scatter and the absorber that satisfy the condition that (1) two events are consecutive, (2) the events in the scatterer and in the absorber are combined, and (3) the time difference of two events is less than 1 µs, are extracted. Subsequently, the time width and channel are converted to the energy and the coordinates, respectively, and the time stamps of two Compton cameras are corrected by using 50 ms external clocks. For the reconstruction of a single Compton camera, these data are used. For the reconstruction of DPECT, moreover, all coincidence events of the two Compton cameras were sorted by the corrected time stamp and subsequently extracted. The extracted coincidence events satisfy the condition that (1) two events are consecutive, (2) the events in camera1 and in camera2 are combined, and (3) the time difference of two events is less than 2 µs.

The image is reconstructed with the algorithm based on the back projection (BP). In the program, coincident events used for the BP reconstruction are selected by energy. Only coincident events in which the sum of the energy detected in the scatterer and absorber is within ± 10 % of the gamma-ray energy of interest, and the two energy is 605 keV and 796 keV, and the energy in the scatterer E_s satisfies following equation, are used.

$$E_s = \frac{E_1}{1 + \frac{2E_1}{m_0c^2}(1 - cos\theta)} \tag{1}$$

Here, E_1 is the gamma-ray energy of interest, m_0 is the electron rest mass and c is the light speed, and the θ is the Compton scattering angle. We used the value of E_s calculated from the experimental geometry. Although back scattering events occur (gamma-ray is scattered in the absorber and absorbed in scatterer), discriminating between the Compton scattering and the back scattering is difficult in this system. Therefore, the energy in the scatterer is also limited to eliminate back scattering events.

Compton cones are blurred and drawn using Eq.(2) with the value of angular resolution measure (ARM) because the resolution of a detector is limited. The ARM is used as the index of an angular resolution of the Compton camera and defined in Eq.(3). In this study, the value of 12° is used as the ARM of the two Compton cameras.

$$Gaussian(\omega, \theta, ARM) = exp\left(-0.5 \times \left[\frac{\omega - \theta}{ARM/2.35}\right]\right) \tag{2}$$

$$ARM = \theta_e - \theta_g \tag{3}$$

Here,ω is the angle between the cone axis and the direction vector from the scattering position to an image pixel, and θ is the Compton scattering angle calculated from the energy. θ_e is the Compton scattering angle calculated from the detected energy in the scatterer and absorber, and θ_g is the Compton scattering angular calculated from the position of the source and the position where the Compton scattering event occurred. For the reconstruction of DPECT, Eq.(4) is used. The value that is normalized by the sum of the value of the each pixel for each event is added to the pixel.

$$exp\left(-0.5 \times \left[\frac{(\omega_1 - \theta_1)^2 + (\omega_2 - \theta_2)^2}{(ARM/2.35)^2}\right]\right) \tag{4}$$

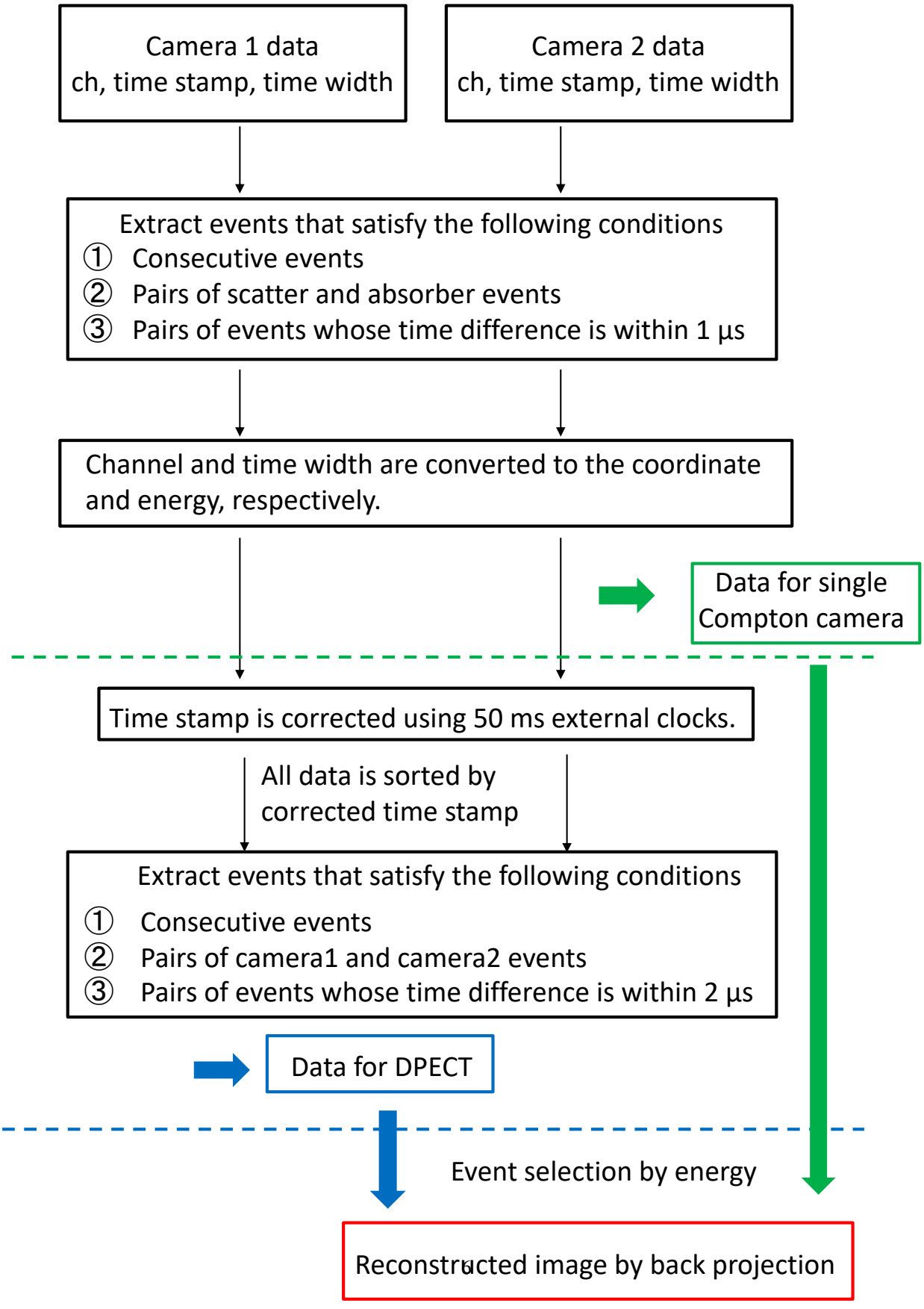

Figure 4: Data analysis flow.

3. Results

3.1. Imaging of point source of ^{134}Cs

First, we demonstrated the DPECT method with the point source of ^{134}Cs. ^{134}Cs (755 kBq), placed in the center between camera1 and camera2 (see Fig.3). The measurement time was 120 minutes. The reconstructed images of a single Compton camera are shown in Fig.5. The left figure (a) is the image reconstructed by using the Compton events of 605 keV gamma-ray and the right figure (b) is the image reconstructed by using the that of 796 keV gamma-ray. Figure 6 shows the reconstructed image of DPECT (605 keV and 796 keV). These figures show that the background in the image of DPECT is reduced compared with the images of a single Compton camera. The reconstructed image of DPECT is clearer. Figure 7 shows the Z-X and Y-Z cross section of the hot spot for the single Compton imaging and DPECT, and Figure 8 shows the 3-D image plot of DPECT and a single Compton by using 605 keV.. The base line of the DPECT imaging was reduced. Each of the spatial resolution and SNR is shown in Table 1. The number of events used for the reconstruction of DPECT was more than 1000 times less than that of a single Compton imaging. This low efficiency of DPECT was similar with the simulation [10]. The spatial resolution of the peak point of DPECT is not improved by much. However, the SNR of DPECT was improved by approximately more than 1.5 times.

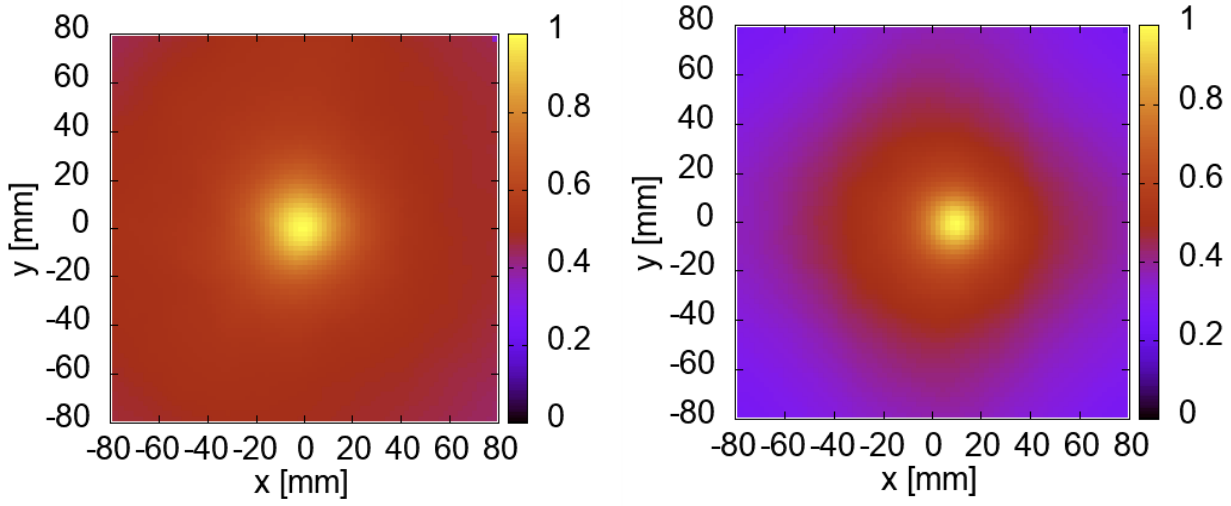

(a) The reconstructed image using 605 keV

(b)The reconstructed image using 796 keV

Figure 5: The ^{134}Cs reconstructed images of single Compton

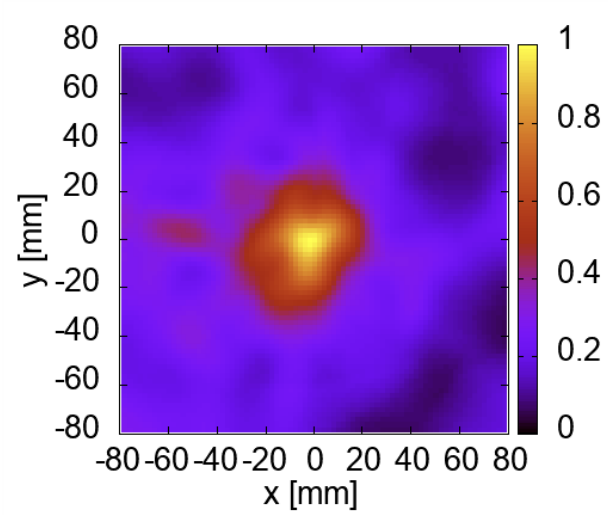

Figure 6: The ^{134}Cs reconstructed images of DPECT

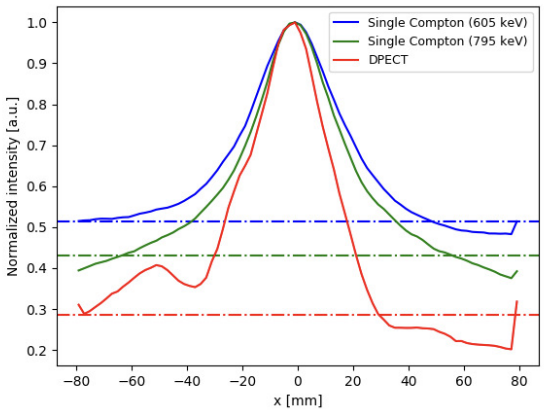

(a) The Z-X cross section of the hot spot.

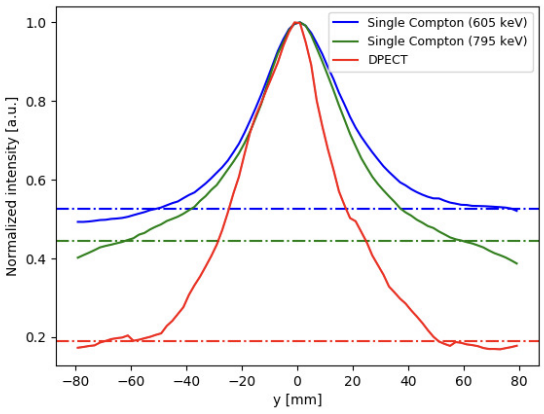

(b)The Y-Z cross section of the hot spot.

Figure 7: The cross section of the peak point for each reconstructed images of ^{134}Cs.

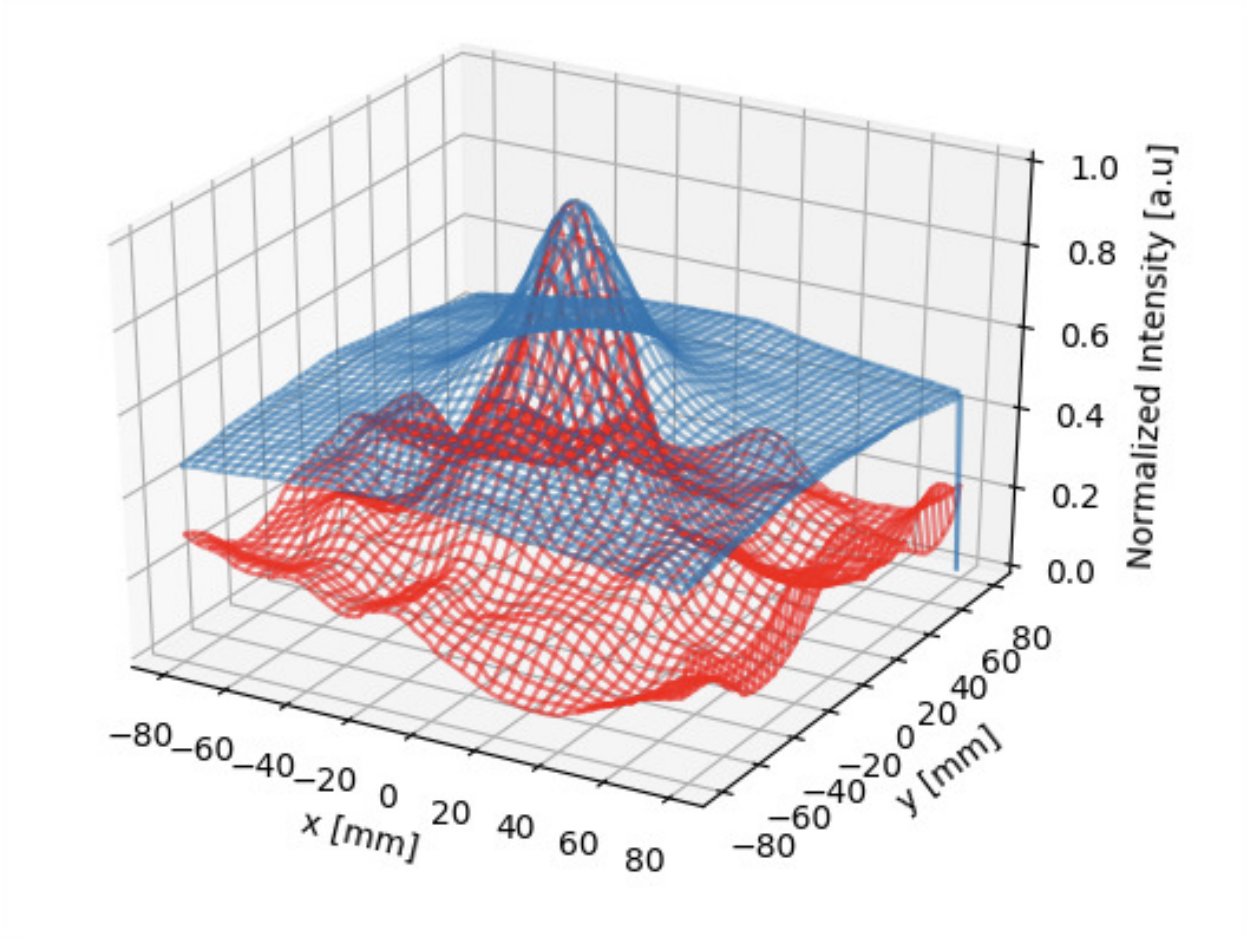

Figure 8: The 3D plot of the ^{134}Cs reconstructed images of DPECT. The red one is the 3D image plot of DPECT, and the blue one is the that of a single Compton by using 605 keV.

Table 1: The evaluation of the peak point in the reconstructed image for ^{134}Cs point source

	single Compton (605 keV)	single Compton (796 keV)	DPECT (796-605 keV)
event number	776846	456571	291
spartial resolution (x,y) [mm]	(39.5,39.1)	(40.2,42.1)	(33.5, 42.0)
SNR (x,y)	(1.89,1.85)	(2.23,2.16)	(3.38,4.86)

3.2. Imaging of point source of ^{134}Cs in the background by ^{137}Cs

We also demonstrated the imaging of the point source of ^{134}Cs (674 kBq) in the background of ^{137}Cs (998 kBq). ^{134}Cs was placed in $(x, y, z) = (10, 0, 60)$ [mm], while ^{137}Cs was placed in $(x, y, z)=(-40, -30, 0)$ [mm]. The measurement time was 120 minutes. The reconstructed images of single Compton camera and DPECT are shown in Fig.9 and 10, respectively. Figure 9 (a) is the image reconstructed using the Compton events of a 605 keV gamma-ray and Figure 9 (b) is the image reconstructed using the Compton events of a 796 keV gamma-ray. In Figure 9 (a), the peak point of 662 keV gamma-ray from ^{137}Cs source is also shown. The energy resolution of the two cameras is

approximately 12 % for 662 keV. The coincidence events in which the sum of the energy detected in the scatterer and the absorber is within ± 10 % of the gamma-ray energy of interest, were used for the reconstruction. Therefore, in the reconstruction of single Compton by using 605 keV, the coincidence events contained events of the 662 keV. Compared with the reconstruction images of a single Compton, the image of DPECT shown in Fig.9 is clearer and has little background of ^{137}Cs. Figure 11 shows the Z-X and Y-Z cross section of the hot spot for the single Compton imaging and DPECT, and Figure 12 shows the 3-D image plot of DPECT and a single Compton by using 605 keV. The base line of the DPECT imaging was reduced. These results show that DPECT can provide a clearer image of the nuclides, which emits two or more gamma-rays, even in the background of gamma-rays whose energy is close to that of the nuclide of interest. The evaluation of these reconstructed images is shown in Table.2. The spatial resolution of DPECT is not significantly different from that of a single Compton. However, the SNR of the x-axis and y-axis of the DPECT is improved by approximately two times.

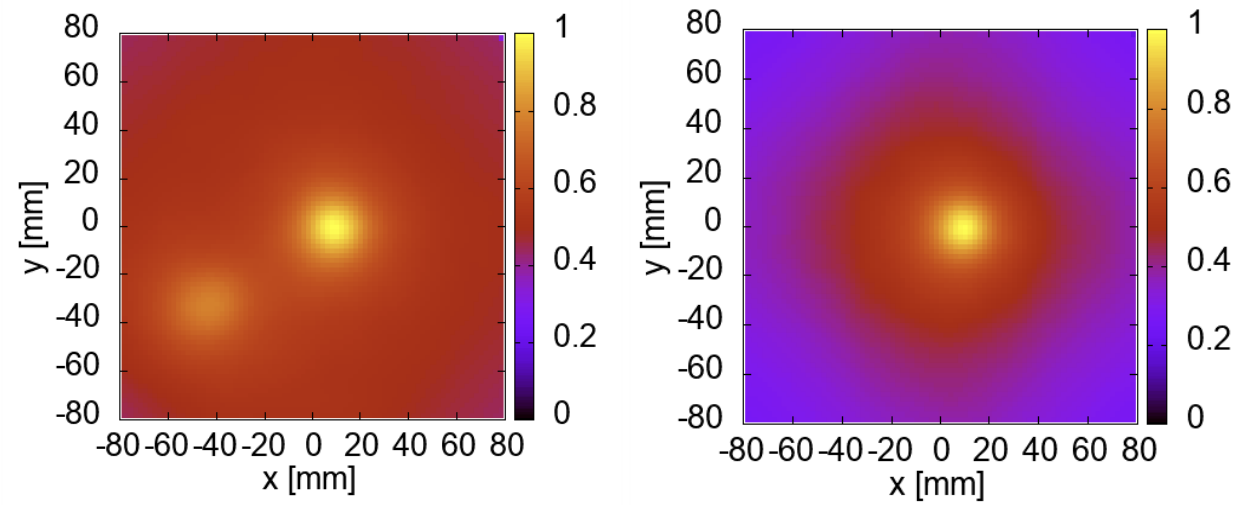

(a) The reconstructed image using 605 keV

(b)The reconstructed image using 796 keV

Figure 9: The ^{134}Cs reconstructed images of single Compton in the background of ^{137}Cs

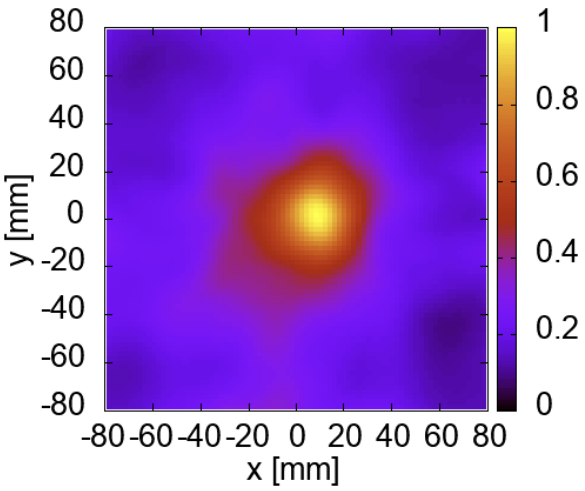

Figure 10: The ^{134}Cs reconstructed images of DPECT in the background of ^{137}Cs

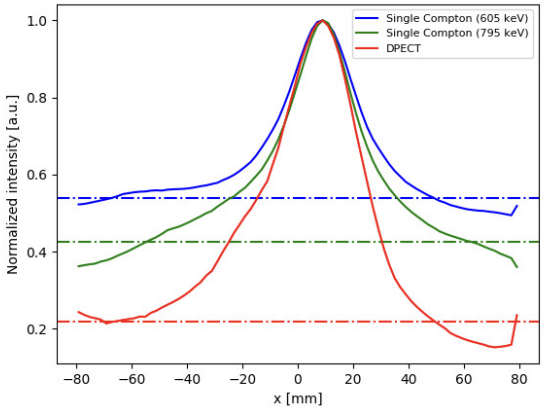

(a) The Z-X cross section of the hot spot.

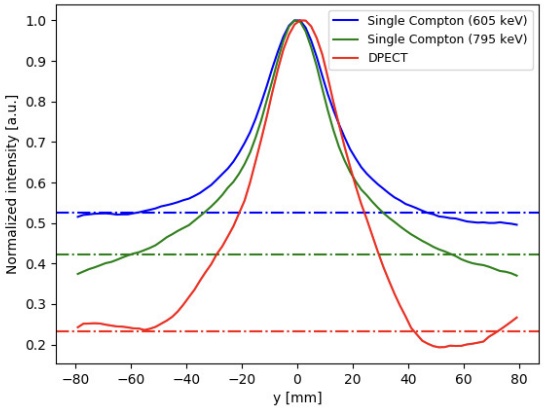

(b)The Y-Z cross section of the hot spot.

Figure 11: The cross section of the peak point for each reconstructed images of ^{134}Cs in the background of ^{137}Cs.

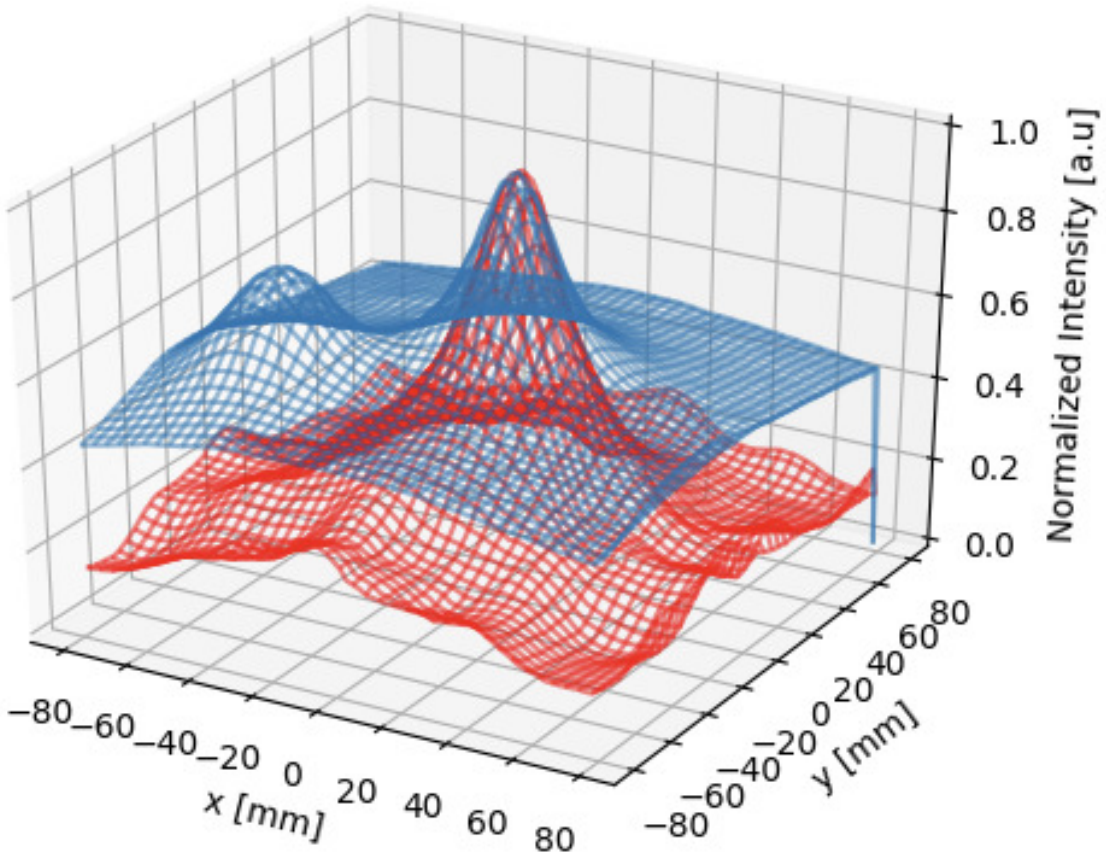

Figure 12: The 3D plot of the ^{134}Cs reconstructed images of DPECT in the background of ^{137}Cs. The red one is the 3D image plot of DPECT, and the blue one is the that of a single Compton by using 605 keV.

Table 2: The evaluation of the peak point in the reconstructed image for ^{134}Cs point source in the background of ^{137}Cs

	single Compton (605 keV)	single Compton (796 keV)	DPECT (796-605 keV)
event number	1541187	804151	1093
spartial resolution (x,y) [mm]	(31.6,32.8)	(36.8,37.0)	(38.7, 39.1)
SNR (x,y)	(1.82,1.83)	(2.20,2.21)	(4.33,4.19)

4. Conclusion and discussion

We demonstrated the DPECT method that utilized the coincidence detection for cascade gamma-rays for the ^{134}Cs imaging with two Ce:GAGG scintillator Compton cameras. The reconstructed images of DPECT became clearer than that of a single Compton for both of the ^{134}Cs point source imaging and the ^{134}Cs point source imaging in the ^{137}Cs background. Moreover, the reconstructed image of DPECT for the ^{134}Cs point source imaging in the ^{137}Cs background

has little background of ^{137}Cs, although the reconstructed image of a single Compton by using 605 keV has the small peak point of 662 keV of ^{137}Cs. The number of events used for the reconstruction of DPECT was more 100 times less than that of a single Compton and the spatial resolution was not improved by much. However, the SNR is improved approximately two times, and these results shows that DPECT is effective for the imaging of the nuclide, which emits two or more gamma-rays, in the background of gamma-rays, of which the energy is close to that of the nuclide of interest.

References

[1] R. W. Todd, J. M. Nightingale, D. B. Everett, A proposed γ camera 251 (1974) 132–134.

[2] J.E.Gormley, W.L.Rogers, N.H.Clinthorne, D.K.Wehe, G.F.Knoll, Experimental comparison of mechanical and electronic gamma-ray collimation, Nucl. Instr. and Meth. A 397 (1997) 440–447.

[3] J. Jiang, K. Shimazoe, Y. Nakamura, H. Takahashi, Y. Shikaze, Y. Nishizawa, M. Yoshida, Y. Sanada, T. Torii, M. Yoshino, et al., A prototype of aerial radiation monitoring system using an unmanned helicopter mounting a GAGG scintillator Compton camera, Journal of Nuclear Science and Technology 53 (7) (2015) 1067–1075.

[4] Y. Shikaze, Y. Nishizawa, Y. Sanada, T. Torii, J. Jiang, K. Shimazoe, H. Takahashi, M. Yoshino, S. Ito, T. Endo, et al., Field test around Fukushima Daiichi nuclear power plant site using improved Ce:$Gd_3(Al,Ga)_5O_{12}$ scintillator Compton camera mounted on an unmanned helicopter, Journal of Nuclear Science and Technology 53 (12) (2016) 1907–1918.

[5] S.Takeda, A.Harayama, Y.Ichinohe, et al., A portable Si/CdTe Compton camera and its applications to the visualization of radioactive substances, Nucl. Instr. and Meth. A 787 (2015) 207–211.

[6] R. Orito, H. Kubo, K. Miuchi, T. Nagayoshi, A. Takada, A. Takeda, T. Tanimori, M. Ueno, Compton gamma-ray imaging detector with electron tracking, Nuclear Instruments and Methods in Physics Research Section A: Accelerators, Spectrometers, Detectors and Associated Equipment 525 (1) (2004) 107 – 113.

[7] K. Vetter, D. Chivers, B. Plimley, A. Coffer, T. Aucott, Q. Looker, First demonstration of electron-tracking based Compton imaging in solid-state detectors, Nuclear Instruments and Methods in Physics Research Section A: Accelerators, Spectrometers, Detectors and Associated Equipment 652 (1) (2011) 599 – 601.

[8] Y.Yoshihara, K.Shimazoe, Y.Mizumachi, H.Takahashi, et al., Development of electron-tracking Compton imaging system with 30-μm SOI pixel sensor, Journal of Instr. 12 (2017) C01045.

[9] H. Yoneda, S. Saito, S. Watanabe, H. Ikeda, T. Takahashi, Development of Si-CMOS hybrid detectors towards electron tracking based Compton imaging in semiconductor detectors, Nuclear Instruments and Methods in Physics Research Section A: Accelerators, Spectrometers, Detectors and Associated Equipment.

[10] Y. Yoshihara, K. Shimazoe, Y. Mizumachi, H. Takahashi, Evaluation of double photon coincidence Compton imaging method with GEANT4 simulation, Nuclear Instruments and Methods in Physics Research Section A: Accelerators, Spectrometers, Detectors and Associated Equipment 873 (2017) 51 – 55.

[11] K. Kamada, S. Kurosawa, P. Prusa, M. Nikl, V. V. Kochurikhin, T. Endo, K. Tsutumi, H. Sato, Y. Yokota, K. Sugiyama, A. Yoshikawa, Cz grown 2-in. size Ce:$Gd_3(Al,Ga)_5O_{12}$ single crystal; relationship between Al, Ga site occupancy and scintillation properties, Optical Materials 36 (12) (2014) 1942 – 1945.

[12] K.Shimazoe, H.Takahashi, B.Shi, T.Orita, T.Furumiya, J.Ooi, Y.Kumazawa, Dynamic Time Over Threshold Method, IEEE Trans. On Nucl. Sci. 59 (6) (2012) 3213–3217.

[13] T. Orita, K. Shimazoe, H. Takahashi, The dynamic time-over-threshold method for multi-channel APD based gamma-ray detectors, Nuclear Instruments and Methods in Physics Research Section A: Accelerators, Spectrometers, Detectors and Associated Equipment 775 (2015) 154 – 161.